Petrologic and thermobarometric study of the Riás schists (NW Iberian Massif)

Byron Ernesto Solís-Alulima[1, 2], Alicia López-Carmona[1, 2, 3], Gabriel Gutiérrez-Alonso[1, 3], Antonio M. Álvarez-Valero[1]

(1) Geology Department; Faculty of Science; University of Salamanca; Plaza de la Merced s/n, 37008, Salamanca, Spain.
sabe@usal.es; alioli@usal.es; aav@usal.es; gabi@usal.es
(2) Mineralogy and Petrology Department; Faculty of Geology; Complutense University of Madrid;
Calle José Antonio Novais, 12, 28040 Madrid, Spain.
(3) Laboratory of Structural Petrology; Faculty of Geology and Geography; Tomsk State University;
36 Lenin Avenue, 634050, Tomsk, Russia.

ABSTRACT

The Riás Schists crop out in the so-called Iberian Variscan parautochthon, surrounding the Malpica-Tui Complex (NW Iberian Massif), as part of the westernmost internal areas of the European Variscan belt. Three Variscan metamorphic events have been identified in the Riás Schists (M_1, M_2 and post-M_2). M_1 comprise unoriented microinclusions that have only been identified in garnet porphyroblast cores and inside staurolite crystals. M_2, comprises the matrix foliation (S_2) and the assemblage $garnet_{RIM}$ + staurolite + muscovite + biotite + chlorite + rutile/ilmenite + magnetite + quartz and the development of syntectonic andalusite. Finally, post-M_2 (post-S_2) includes andalusite and plagioclase together with secondary muscovite, biotite and chlorite and accessory tourmaline, Fe/Ti oxides, apatite and carbonate. Results of multi-equilibrium thermobarometry (pressure-temperature pseudosections), for M_2 indicates a medium-pressure Barrovian metamorphic event (0.5-0.6 GPa; 580-570 °C; *ca.* 20 km deep), followed by moderate cooling during decompression, together with the extensional collapse of the Variscan orogenic pile (post-M_2; 0.3 GPa; 540 °C; *ca.* 10 km deep). Inferred P T conditions in the Riás Schists, and their spatial relationship with the overlying allochthonous high-pressure pelitic schists (i.e. Ceán Schists), suggest that both lithologies were part of the same continental margin during the beginning of the Variscan orogeny. However, they experienced very different tectonothermal evolutions due to their putative locations in the orogenic wedge.

Keywords: Variscan orogeny, P–T pseudosections, pelitic schists, metamorphic reactions balance.

Estudio petrológico y termobarométrico de los esquistos de Riás (NO Macizo Ibérico)

RESUMEN

Los Esquistos de Riás afloran en el parautóctono del orógeno Varisco de Iberia, en el entorno del Complejo de Malpica-Tui (NO del Macizo Ibérico), en el sector interno más occidental de la Cadena Varisca Europea. Se han identificado tres eventos metamórficos en los Esquistos de Riás (M_1, M_2 y post-M_2). M_1 incluye microinclusiones sin orientación preferente que sólo se han identificado en los núcleos de los porfiroblastos de granate y en los cristales de estaurolita. M_2 comprende la foliación principal de la matriz (S_2) y está constituido por la paragénesis $granate_{BORDE}$ + estaurolita + moscovita + biotita + clorita + rutilo/ilmenita + magnetita + cuarzo y el desarrollo de porfiroblastos sintectónicos de andalucita. El evento post-M_2 (post-S_2) incluye andalucita y plagioclasa, además de moscovita, biotita y clorita secundarias y cantidades accesorias de turmalina, óxidos de Fe-Ti y carbonato. Los resultados de las técnicas de termobarometría multiequilibrio (pseudosecciones presión-temperatura), caracterizan M_2 como un evento metamórfico Barroviense de media presión (0.5-0.6 GPa; 580-570 °C; ca. 20 de profundidad) seguido de una exhumación con enfriamiento moderado, coetánea con el colapso extensional de la pila orogénica Varisca (post-M_2; 0.3 GPa; 540 °C; ca. 10 km de profundidad). Las estimaciones realizadas en los Esquistos de Riás, y su relación espacial con los esquistos pelíticos de alta presión del alóctono (i.e. Esquistos de Ceán), sugieren que ambas litologías formaron parte

del mismo margen continental durante el comienzo de la orogenia Varisca, pero experimentaron evoluciones tectonotermales muy distintas por su posición original en la cuña orogénica.

Palabras clave: Orogenia Varisca, pseudosecciones P–T, esquistos pelíticos, balance de reacciones metamórficas.

Introduction

Investigating the metamorphic evolution of the most representative areas of an orogen at a regional scale includes the study of the processes involved in the subduction and exhumation of the terranes that form the suture realm. This is an essential task that aids the deciphering of the evolution of the whole orogenic edifice.

Within this general context, the Riás Schists (Llana-Fúnez, 2001) represent a metasedimentary sequence that experienced intermediate-pressure Barrovian metamorphism (cf. Llana-Fúnez, 2001; Diéz-Fernández, 2011). This sequence is located structurally below a thick sheet of high-pressure (HP) rocks (Rodríguez *et al.*, 2003; López-Carmona *et al.*, 2010; 2013; 2014; Li and Massone, 2016; Puelles *et al.*, 2017). Both units are separated by a tectonic contact interpreted as an east directed thrust (Llana-Fúnez, 2001) or as a top-to-the-west extensional detachment (Diéz Fernández, 2011). However, the metamorphic gap between the Barrovian and the HP metamorphic rocks has not yet been described in detail. This contribution aims to characterize the processes that led to this actual geometry through a comprehensive thermobarometric study using thermodynamic modelling.

The main objective of this study is to decipher the pressure–temperature (P–T) evolution of the Riás Schists and describe the relationship between the two units with distinct metamorphism, within the framework of the collision, and subsequent evolution, of the Variscan orogen in the NW Iberian Massif.

Objetives

The objectives of this contribution include:
- A comprehensive petrological and thermobarometric study of the Riás Schists that crop out in the eastern coastal area of the so-called parauthocthonous terrain, in the vicinity of the Malpica-Tui Allochthonous Complex.
- Establish a detailed P–T path for the pelitic schists in order to characterize their tectonothermal evolution.
- Compare the parautocthonous schists with the allochthonous high-pressure schists from the Ceán Unit (Malpica-Tui Complex).

Geological setting

The Riás Schists (Llana-Fúnez, 2001) outcrop in the so-called Galicia – Trás-os-Montes Zone (Farias *et al.*, 1987; Arenas, 1988), in NW Iberia, in the westernmost sector of the European Variscan Belt.

The Variscan orogen is a vast collision belt formed during the upper Paleozoic (Devonian to Permian) by the convergence and final collision of Gondwana and Laurussia, giving rise to the last supercontinent, Pangea. This collision is commonly interpreted to have involved several microplates located in an intermediate position, known as peri-Gondwana terrains. These terranes were amalgamated over Gondwana during the Devonian-Carboniferous, generating a large orogenic wedge prior to its final accretion with Laurussia (von Raumer and Stampfli, 2008; Martínez Catalán *et al.*, 2009). The suture zone of this collision, where the remnants of consumed oceanic lithosphere are preserved, is currently represented in the so-called Allochthonous Complexes, scattered throughout the different European Variscan Massifs.

During the Paleozoic, the Iberian Peninsula was located near the confluence of the three most important Paleozoic orogenic belts: Apalachian, Caledonian and Variscan. For this reason, the sector of the Variscan orogen that outcrops in NW Iberia is one of the key geological places to study the Precambrian and Paleozoic evolution of the Earth (e.g. Martínez Catalán *et al.*, 2002).

The Galicia – Trás-os-Montes Zone (Fig. 1; GTOMZ; Farias *et al.*, 1987; Arenas, 1988) constitutes a large allochthonous sheet superimposed over the Central Iberian Zone (CIZ; Julivert *et al.*, 1972; 1980) and comprises (i) the structurally lower Schistose Domain (Farias *et al.*, 1987) and (ii) the upper Allochthonous Complexes (Arenas, 1988).

The Schistose Domain includes a thick sequence (*ca*. 7-8 km) of siliciclastic metasediments and felsic metavolcanic rocks, Ordovician-Devonian in age, interpreted as a section of the northernmost outward continental margin of Gondwana during the Paleozoic, tectonically transported into the innermost areas of the Variscan orogen (Martínez Catalán *et al.*, 2009).

Although the Paleozoic sequence of the Schistose Domain and the CIZ show different characteristics, their stratigraphy and their similar variscan
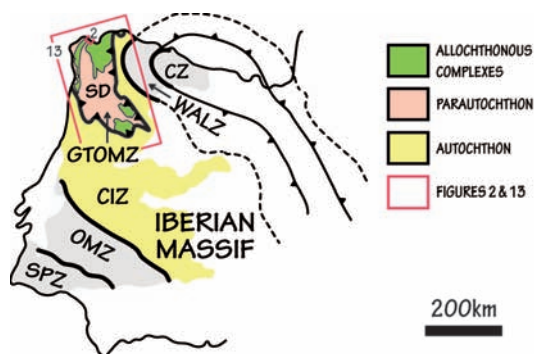
Figure 1. Distribution of the different domains of the Iberian Massif (simplified from Julivert *et al.,* 1972; Farias *et al.,* 1987; Martínez Catalán *et al.,* 2002). CZ-Cantabrian Zone; WALZ-Asturoccidental-Leonese Zone; SD-Schistose Domain; GTOMZ-Galicia – Trás-os-Montes Zone; CZI-Central Iberian Zone; OMZ-Ossa-Morena Zone; SPZ- South Portuguese Zone.
Figura 1. Distribución de los diferentes dominios del Macizo Ibérico (simplificada de Julivert et al., 1972; Farias et al., 1987; Martínez Catalán et al., 2002). CZ-Zona Cantábrica; WALZ-Zona Asturoccidental Leonesa; SD-Dominio Esquistoso; GTOMG-Zona de Galicia –Trás-os-Montes; CIZ-Zona Centro Ibérica; OMZ-Zona de Osa Morena; SPZ-Zona Sur Portuguesa.

tectonothermal history, suggest a close paleogeographic relation (Marquínez-García, 1984; Farias *et al.,* 1987; Díaz García, 1992; Dallmeyer *et al.,* 1997, Murphy and Gutierrez-Alonso, 2008; Dias da Silva *et al.,* 2012). For this reason, the Schistose Domain cannot be considered an exotic terrain and therefore, would constitute the relative autochthon, or parautochthon (Ribeiro *et al.,* 1990), when compared with the Allochthonous Complexes. In this contribution, the nomenclature proposed by Ribeiro *et al.* (1990) will be used.

The Allochthonous Complexes consist of a succession of units with different affinities that underwent large displacements, which were thrusted over the Schistose Domain and became part of a large nappe stack during the Variscan collision (Ries and Shackeleton, 1971; Martínez Catalán *et al.,* 2007; Arenas *et al.,* 2016). The succession of allochthonous units is interpreted as terranes formed in a different palaeogeographic settings during Cambrian to Devonian times, including continental margins (lower allochthon), consumed oceanic areas (middle allochthon) and magmatic arcs (upper allochthon). After experiencing a polyphase Varican tectonothermal evolution, intense thinning and a strong dismemberment of the original pile, the evolution of the Allochthonous Complexes culminated with the exhumation of their units (cf. Martínez Catalán *et al.,* 2002; Gómez Barreiro *et al.,* 2007; Díez Fernández *et al.,* 2011). Currently, they represent residual mega-klippen

of the initial stack, preserved in late synforms exposed in the NW Iberian Massif of Spain (Cabo Ortegal, Órdenes and Malpica-Tui Complexes) and Portugal (Bragança and Morais Complexes), as well as in different massifs across Brittany and central and western Europe.

Study area

The parautochthon (PA; Ribeiro *et al.,* 1990) in the coastal section of the Malpica-Tui Complex (MTC; Rodríguez, 2005) displays very limited outcrops compared to other areas of the GTOMZ (Fig. 2). To the east, the PA and the MTC are separated by a basal shear zone (Gil Ibarguchi and Ortega Gironés, 1985). This contact is interpreted as a thrust to the east (Llana-Fúnez, 2001) or as an extensional detachment to the west (Díez Fernández, 2011). To the west, a late Variscan dextral sub-vertical strike-slip shear zone (named Malpica-Lamego Shear Zone, *ca.* 310 Ma, Gutiérrez-Alonso *et al.,* 2015) limits both units (Coke and Ribeiro, 2000; Llana-Fúnez, 2001).

In the vicinity of the MTC, three cartographic units have been distinguished in the PA (cf. Alonso and González, 1982; Díez Fernández, 2011): (i) medium grade schists, whose most representative outcrop is located to the east of the MTC, from the Riás Beach to Chan de Razo Cape (Figs. 2 and 3); (ii) the para-derived high-grade migmatites, which are best found in the vicinity of the Mount Neme and (iii) the glandular orthogneisses that outcrop to the west of the MTC, in the San Adrián Cape, and in the coastal section of the southern margin of the *Ría de Arousa.* The limit between the schists and the migmatites is interpreted as a metamorphic isograd, evidenced by a notable increase in the micas size due to increasing temperature during the main fabric generation (Díez Fernández, 2011). Traditionally, the first two units, of sedimentary origin, have been attributed to the Paraño Group of the Schistose Domain of the GTOMZ (Alonso and González, 1982; Marquínez García, 1984).

The study area includes the westernmost outcrops of the Riás Beach, located to the southeast of Malpica de Bergantiños (A Coruña, Galicia; Fig. 2), on the popularly known *Costa da Morte.*

The most characteristic stratigraphic sequence of the parautochthon in the studied area, from the structurally lower levels to the upper ones, can be recognized from Chan de Razo Cape to the Riás Beach, respectively. This sequence includes fine-grained siliciclastic rocks metamorphosed to micaschists and interbedded metasandstones, black metasiliceous rocks (lydites) and graphite-rich schists (Fig. 3). In the
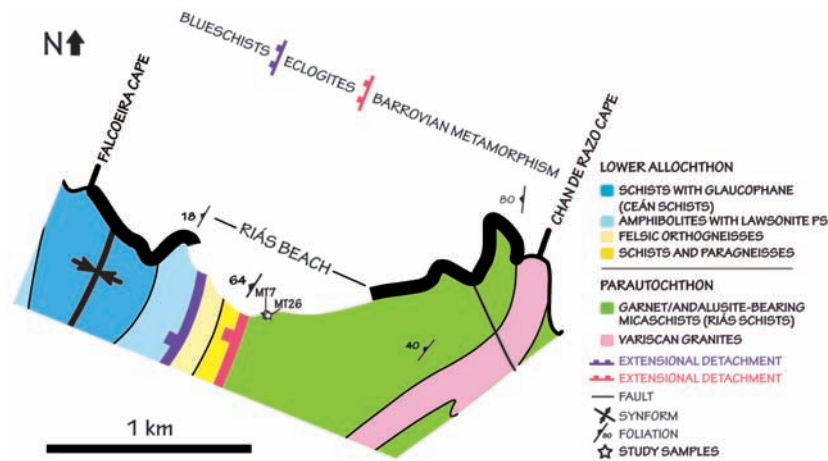
Figure 2. Simplified geological map of the study area (modified from López-Carmona, 2015). PS: pseudomorph.
Figura 2. *Mapa geológico simplificado de la zona de estudio (modificado de López-Carmona, 2015). PS: pseudomorfo.*

highest part the sequence (which is the aim of this study) the studied rocks depict a stretching lineation developed on the schistosity planes. The main foliation observed in the studied rocks is a tectonic banding defined by alternating quartz ribbons (mm to cm thick) and mica-rich domains, which include syntectonic andalusite (sample MT26) and occasional garnet (sample MT7). Frequently, decimetric to metric quartzite levels with a little lateral continuity and quartz veins are present. Sub-vertical to steep west-dipping folds, with associated crenulation cleavage, affect the main foliation and the stretching lineation. Isoclinal folds appear when appropriate markers with high competence contrast are present. Throughout all the metamorphic sequence, metric to decametric-scale boudins and bodies of leucogranite are frequent (cf. Llana-Fúnez, 2001; Díez Fernández, 2011; Fig. 3)

Methodology

The methodology applied to attain the proposed objectives include:

- Bibliographic review of the GTOMZ, focused in the Schistose Domain and the field review of the published geological maps at 1:50000 (Hoja n° 44, Sisargas-Carballo; Alonso and González, 1982; Serie MAGNA del Instituto Geológico y Minero de España) and 1:25000 scales (Geological Map of the Malpica-Tui Complex; Díez Fernández, 2011).
- And the following analytical techniques:
  - Optical microscopy involved the comprehensive petrographic study, including the blastesis-deformation relations, and was
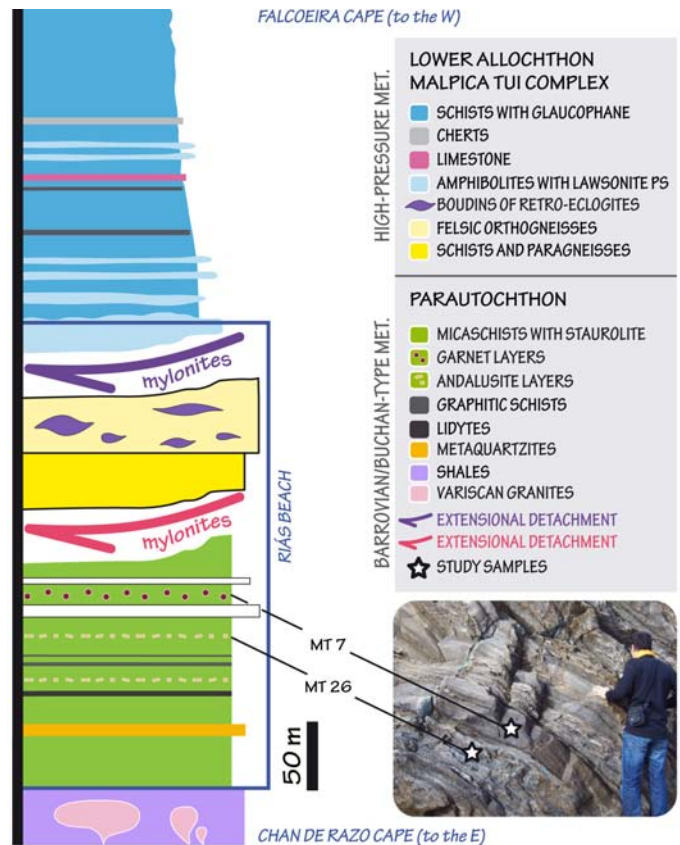

Figure 3. Idealized lithostratigraphic column of the study area which includes the coastal section between Chan de Razo Cape and Falcoeira Cape (location of the outcrop: N43°17'35.88", W8°44'38.65"; modified from Llana-Fúnez, 2001; López-Carmona et al., 2014). PS: pseudomorph.
Figura 3. *Columna litoestratigráfica idealizada de la zona de estudio que abarca la sección costera entre la Punta de Chan de Razo y la Punta da Falcoeira (localización del afloramiento:* N43°17'35.88", W8°44'38.65"; *modificado de Llana-Fúnez, 2001; López-Carmona et al., 2014). PS: pseudomorfo.*

carried out using a transmitted light micro-scope (Nikon ECLIPSE 50i POL) to explore two representative thin sections of the Riás Schists, samples MT7 and MT26.

- The mineral chemistry study included quantitative analysis and X-ray mapping of the minerals with thermobarometric interest, through an electron probe micro-analyzer (EPMA). Analyses were performed at the ICTS – *Luis Bru National Electronic Microscopy Center* at the Complutense University of Madrid with a JEOL-Superprobe JXA-8900M microprobe equipped with five spectrometers. The operating parameters for punctual analyses were 15 kV accelerating voltage, 20 nÅ beam current, between 1 and 5 m beam diameter (1 m for the microinclusions) and 10 ms counting time. X-ray maps were operated at 20 kV, 20 ms and 150 nÅ, in variable areas according to the dimensions of the phases of interest. Mineral abbreviations used in this paper correspond to the final terms of the mineral phases described in the internally consistent database proposed by Holland and Powell (1998; 2003; 2011; http://www.metamorph.geo.unimainz.de/thermocalc/documentation/abbreviations/index.html).

- Mineral formulas, cationic relationships and numerical proportions required for the characterization of the different phases were performed through (i) in-house built specific spreadsheets and (ii) using the AX software (Holland and Powell, 2000 in Powell and Holland, 2002; http://www.esc.cam.ac.uk/research/researchgroups/research-projects/tim-hollands-software-pages/ax). The estimation of Fe^{3+} has been calculated stoichiometrically.

- The balance of metamorphic reactions to estimate the effect of changes in chemical composition in an equilibrated micro-domain was implemented by solving systems of linear equations using an in-house built spreadsheet.

- Whole rock analysis of the rock slabs used to make the thin sections from the most representative samples of the Riás Schists were performed by X-ray fluorescence spectrometry (XRF) in *Activation Laboratories Ltd.* (Actlabs, Canada, http://www.actlabs.com). FeO_T is obtained as Fe_2O_3. The proportion FeO (*vs*. Fe_2O_3) was determined by wet chemical titration. The expression that allows us to obtain the Fe_2O_3 ratio is $[(FeO_T/1.43) - (FeO/1.286)] * 1.43$.

- Multi-equilibrium thermobarometry was performed using Theriak-Domino software (de Capitani and Brown, 1987), version: 04.02.2017 (last major modifications: 27 July 2016).

Results

Petrography, whole rock geochemistry and mineral chemistry

The Riás Schists show a chemical composition of typical pelites (Fig. 4; e.g. Atherton and Brotherton, 1982) and a medium grained porphyro-lepidoblastic texture. Quartz and planar minerals constitute more than the 50% (up to 80% in MT7) of the modal proportion of the studied samples. In addition, andalusite ($\approx$ 40%; MT26), plagioclase ($\approx$ 20%), garnet ($\approx$ 15%; MT7), staurolite ($\approx$ 10%), ilmenite (<5%) and accessory magnetite, tourmaline, carbonates and apatite (<2 %) are observed. A selection of the most representative chemical analyses of the phases described is included in Table 1.
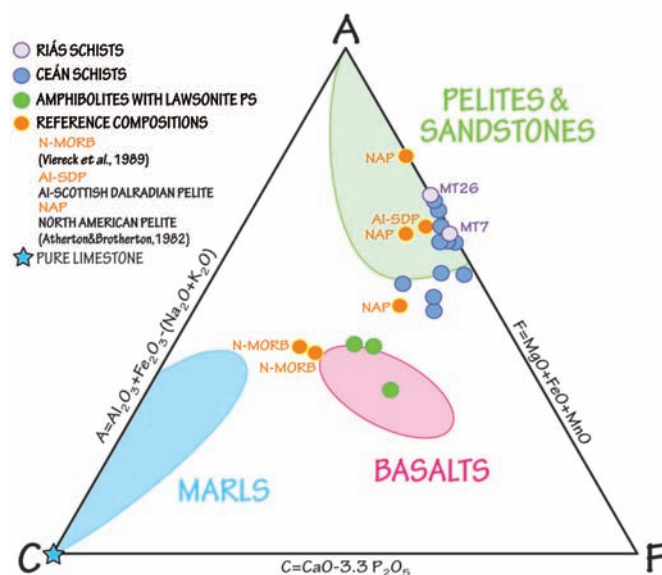

Figure 4. ACF diagram showing the whole rock compositional variations in the studied samples (MT7 and MT26; modified from Turner, 1981; Vernon and Clarke, 2008; López-Carmona, 2015). PS: pseudomorph.
Figura 4. Diagrama ACF en el que se muestra la variación composicional de los análisis de roca total de las muestras estudiadas (MT7 y MT26; modificado de Turner, 1981; Vernon y Clarke, 2008; López-Carmona, 2015). PS: pseudomorfo.

SAMPLE / PHASE	st	ru/ilm	g1 (core)	g1 (rim)	mu	bi	st	chl	and	ilm	pl	g2(core)	g2(rim)	chl	mu	ilm	pl	bi
	*S1 MT26		MT7		S2 MT26					MT7				Post-S2 MT26				MT7
ANALYSIS	13	14	60	70	223	224	213	217	21	202	206	86	81	212	30	14	201	203
SiO_2	26.87	0.03	35.91	36.28	44.62	32.42	26.54	23.03	35.21	0.01	65.78	35.06	36.03	21.99	44.32	0.03	65.17	37.04
TiO_2	0.84	52.99	0.15	0.10	0.28	1.26	0.54	0.09	0.02	53.47	0.00	0.05	0.03	0.07	0.31	52.99	0.01	1.35
Al_2O_3	57.26	0.06	21.40	21.84	38.23	20.92	57.24	24.56	64.24	0.03	20.48	22.81	21.96	25.94	37.54	0.06	20.12	19.54
Cr_2O_3	0.00	0.00	0.00	0.00	0.00	0.00	0.00	0.00	0.00	0.00	0.00	0.00	0.00	0.00	0.00	0.00	0.00	0.00
Fe_2O_3	0.00	0.00	0.00	0.00	0.00	0.40	0.00	0.00	0.00	0.00	0.28	0.00	0.00	0.00	0.00	0.00	0.13	0.00
FeO	9.70	41.44	19.41	23.18	0.67	22.31	10.49	30.30	0.34	39.30	0.00	26.17	29.38	28.92	1.01	41.44	0.00	19.20
MnO	0.57	2.65	21.19	17.38	0.01	0.19	0.40	0.32	0.04	5.95	0.00	13.18	10.71	0.31	0.04	2.65	0.03	0.13
MgO	0.44	0.03	0.73	0.93	0.30	6.55	0.58	8.97	0.03	0.01	0.00	1.10	1.74	8.68	0.38	0.03	0.00	7.55
CaO	0.00	0.01	1.53	1.30	0.04	0.07	0.01	0.05	0.01	0.02	0.30	1.39	0.94	0.01	0.04	0.01	0.59	0.07
Na_2O	0.08	0.00	0.01	0.01	1.08	0.13	0.10	0.04	0.03	0.01	11.99	0.04	0.00	0.03	0.96	0.00	11.49	0.06
K_2O	0.00	0.00	0.00	0.01	9.88	8.77	0.01	0.09	0.00	0.07	0.06	0.00	0.00	0.09	10.07	0.00	0.06	9.01
SUM	95.76	97.21	100.33	101.03	95.11	93.02	95.91	87.45	99.90	98.87	9.89	99.79	100.79	86.04	94.67	97.21	97.60	93.95
OXYGENS	46.00	3.00	12.00	12.00	11.00	11.00	46.00	14.00	5.00	3.00	8.00	12.00	12.00	14.00	11.00	3.00	8.00	11.00
Si	7.46	0.00	2.926	2.931	2.96	2.57	7.39	2.50		0.00	2.92	2.855	2.906	2.42	2.97	0.00	2.93	2.83
Ti	0.18	1.02	0.009	0.006	0.01	0.08	0.11	0.01		1.02	0.00	0.003	0.002	0.01	0.02	1.02	0.00	0.08
Al	18.75	0.00	2.056	2.080	2.99	1.96	18.79	3.15		0.00	1.07	2.190	2.088	3.36	2.96	0.00	1.07	1.76
Cr	0.00	0.00	0.000	0.000	0.00	0.00	0.00	0.00		0.00	0.00	0.000	0.000	0.00	0.00	0.00	0.00	0.00
Fe^{3+}	0.00	0.00	0.075	0.048	0.00	0.02	0.00	0.00		0.00	0.01	0.101	0.096	0.00	0.00	0.00	0.01	0.00
Fe^{2+}	2.25	0.89	1.247	1.518	0.04	1.48	2.44	2.76		0.83	0.00	1.681	1.886	2.66	0.06	0.89	0.00	1.23
Mn	0.13	0.06	1.463	1.189	0.00	0.01	0.10	0.03		0.13	0.00	0.909	0.732	0.03	0.00	0.06	0.00	0.01
Mg	0.18	0.00	0.089	0.112	0.03	0.78	0.24	1.45		0.00	0.00	0.133	0.209	1.42	0.04	0.00	0.00	0.86
Ca	0.00	0.00	0.134	0.113	0.00	0.01	0.00	0.01		0.00	0.01	0.121	0.081	0.00	0.00	0.00	0.03	0.01
Na	0.04	0.00	0.002	0.002	0.14	0.02	0.05	0.01		0.00	1.03	0.006	0.000	0.01	0.13	0.00	1.00	0.01
K	0.00	0.00	0.000	0.001	0.84	0.89	0.00	0.01		0.00	0.00	0.000	0.000	0.01	0.86	0.00	0.00	0.88
SUM	29.01	1.98	8.000	8.000	7.02	7.81	29.12	9.92		1.98	5.04	7.999	8.000	9.91	7.03	1.97	5.04	7.67

Table 1. Representative chemical analyses of the mineral phases described in the Riás Schists.*Micro-inclusions identified as S1 do not show a preferred orientation. Therefore S1 may not refer to a foliation. The same term is maintained to unify the nomenclature.
Tabla 1. Análisis químicos representativos de las fases minerales descritas en los esquistos de Riás. *Las microinclusiones identificadas como S1 no muestran una orientación preferente. Por tanto S1 puede no referirse a una foliación. Se mantiene el mismo término para unificar la nomenclatura.

The studied samples represent the two most characteristic lithological types of the metasedimentary sequence (Figs. 3 and 5). G*arnet-bearing micaschists* (MT7) are the least abundant lithological type and outcrop a few metres from the basal shear zone that separates the PA and the MTC. This sample is an aluminous metapelite (26.34% Al_2O_3) rich in FeO_T (8.75%). A*ndalusite-bearing micaschists* (MT26) appear structurally below the garnet-bearing micaschists and are calcium-poor metapelites (CaO = 0.06%). This chemical/mineralogical variation may be due to compositional differences in their respective protoliths, or because each lithology underwent a different metamorphic evolution due to their putative distinct location in the original pile. Nonetheless, currently both samples appear side by side and interbedded without apparent lithological change at the outcrop scale. Moreover, levels with garnet or staurolite + andalusite are scarce, and are concentrated near the shear zone bounding this unit, in parallel layers that are centimetres apart from each other (Fig. 3). In this outcrop no

evidence has been found that suggests that both samples could be located at different structural levels.

Both samples show a sub-parallel mineralogical banding formed by alternating phyllosilicates (muscovite, biotite and chlorite) and quartz, which gives the rock a planar-planolinear fabric and define the main foliation, which is interpreted to be a S_2 schistosity (Fig. 5).

The first deformation event registered in this lithology is interpreted to be a relict S_1, defined by inclusions of small sized minerals, out of the microprobe beam resolution, within the core of garnet porphyroblasts (quartz and rutile needles) and staurolite crystals (quartz and unrecognized phases).

The main fabric present in the matrix has been described as a S_2 foliation that includes the rim of the garnet porphyroblasts, staurolite, muscovite, biotite, rutile partially/or completely replaced into ilmenite, magnetite, chlorite and quartz, together with the development of syntectonic andalusite. Finally, the post-S_2 foliation includes andalusite and plagioclase
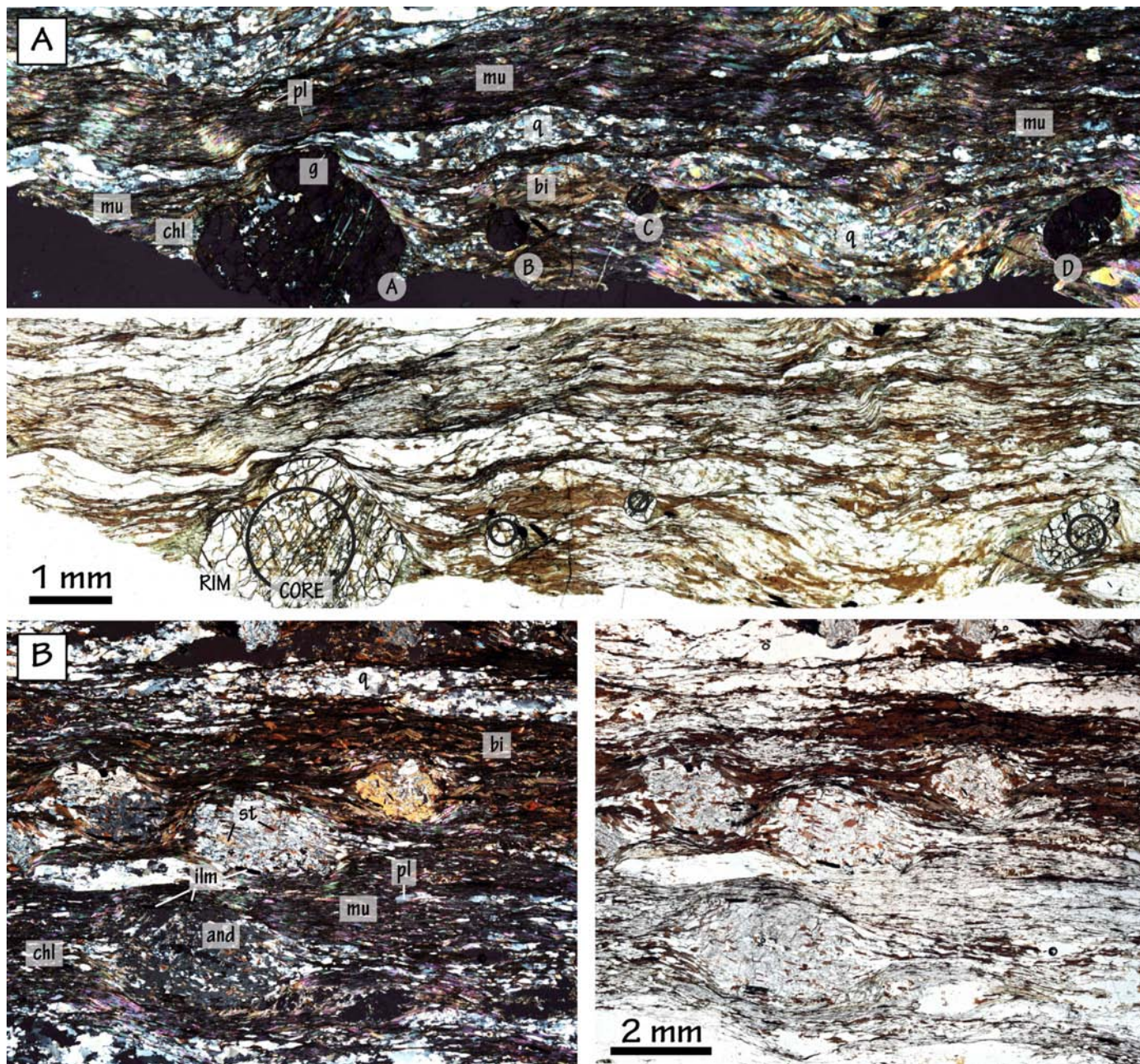
Figure 5. Microphotographs showing the most representative textures and microstructures of the Riás Schists. (A) Garnet-bearing micaschist (MT7); (B) Andalusite-bearing micaschist (MT26).
Figura 5. Microfotografías mostrando las texturas y microestructuras más representativas de los Esquistos de Riás. (A) Micaesquisto con granate (MT7); (B) Micaesquisto con andalucita (MT26.

among secondary muscovite, biotite, chlorite, quartz and accessory tourmaline, Fe/Ti oxides, apatite and carbonate. Post-S_2 foliation is associated with the aforementioned crenulations and is characterized by the presence of C' shear bands affecting S_2, symmetrical pressure tails and shadows, quartz ribbons and mica fish (Fig. 5A). Figure 6 includes a comprehensive

summary of the relationship between the observed deformation phases, metamorphic events, fabrics and parageneses as well as the blastesis-deformation relationships present in the studied samples.

Garnet is only present in sample MT7 and forms sub-idiomorphic porphyroblasts (Fig. 5A). The larger ones (> 1 mm) show two textural domains, a core,
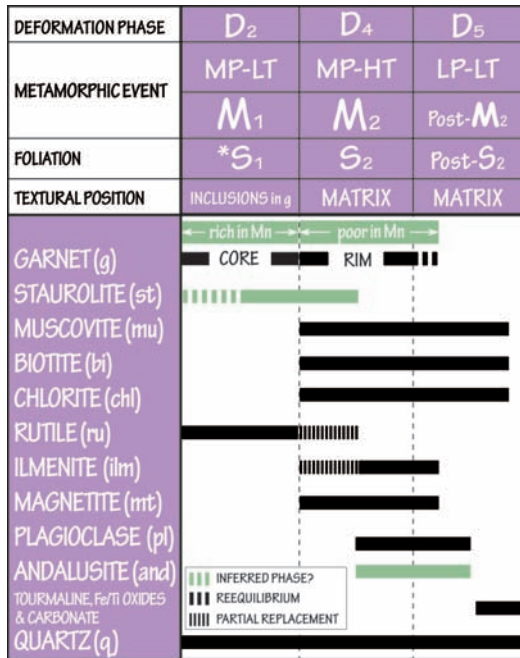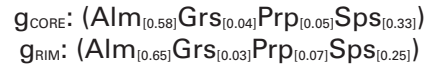
Figure 6. Schematic representation of blastesis-deformation relations in the Riás Schists. *Micro-inclusions identified as S_1 do not show a preferred orientation in these samples. Therefore S_1 may not refer to a foliation. The same term is maintained to unify the nomenclature.

*Figura 6. Representación esquemática de las relaciones blástesis–deformación en los Esquistos de Riás. * Las microinclusiones identificadas como S_1 no muestran una orientación preferente en estas muestras. Por tanto S_1 puede no referirse a una foliación. Se mantiene el mismo término para unificar la nomenclatura.*

associated with S_1, limited by quartz crystals arranged around the central area of the porphyroblasts, and a highly fractured rim, associated with S_2 and partially replaced by chlorite (Fig. 7).

The structural formula of garnet was calculated based on 8 cations. The final terms have been defined based on Deer *et al.*, (1992) and expressed as a mole fraction of almandine (X_{Alm}; X_{Fe}), grossular (X_{Grs}; X_{Ca}), pyrope (X_{Prp}; X_{Mg}) and spessartine (X_{Sps}; X_{Mn}). The average composition of the final terms are:

$$g_{CORE}: (Alm_{[0.58]}Grs_{[0.04]}Prp_{[0.05]}Sps_{[0.33]})$$
$$g_{RIM}: (Alm_{[0.65]}Grs_{[0.03]}Prp_{[0.07]}Sps_{[0.25]})$$

Garnet porphyroblasts show normal zoning patterns and typical growth zoning profiles. From core to rim, show a decrease in spessartine and grossular contents, with maximum values in the core ($X_{Mn}=0.49$, $X_{Ca}=0.05$) and minimum at the rim ($X_{Mn}=0.18$, $X_{Ca}=0.01$). Almandine and pyrope remain constant in the core ($X_{Fe}=0.61$, $X_{Mg}=0.05$) and reaches the maximum towards the rims ($X_{Fe}=0.72$, $X_{Mg}=0.08$). The ratio Fe/(Fe+Mg) reaches its maximum in the core (0.94) and slightly decreases in the rim (to a minimum of 0.89; Fig. 7).

The bell-shaped morphology of the curve that represents the content of spessartine in garnets (bell-shaped profile; Hollister, 1966; Atherton, 1968; Tracy, 1982; Fig. 8) indicates that the core of the porphyrob-
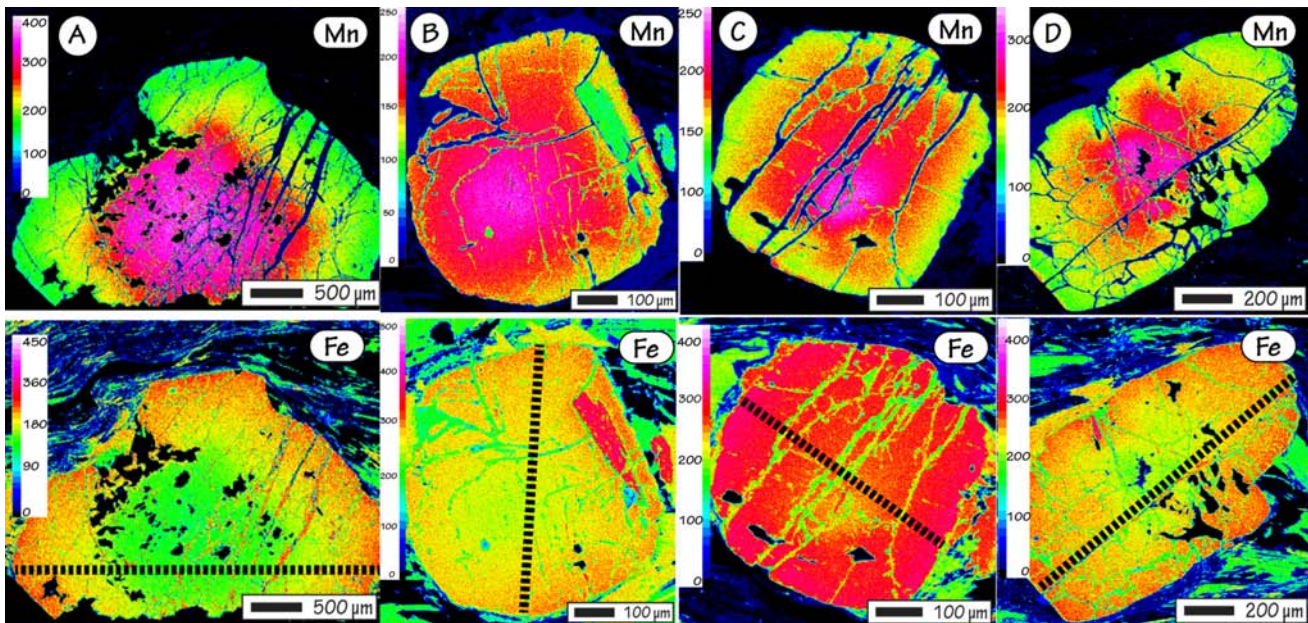

Figure 7. XRF maps of garnet porphyroblasts in the Riás Schists. Dashed lines indicate the location of the chemical profiles.
Figura 7. Mapas XRF de los porfiroblastos de granate de los Esquistos de Riás. Los trazosdiscontinuos señalan la localización de los perfiles químicos.
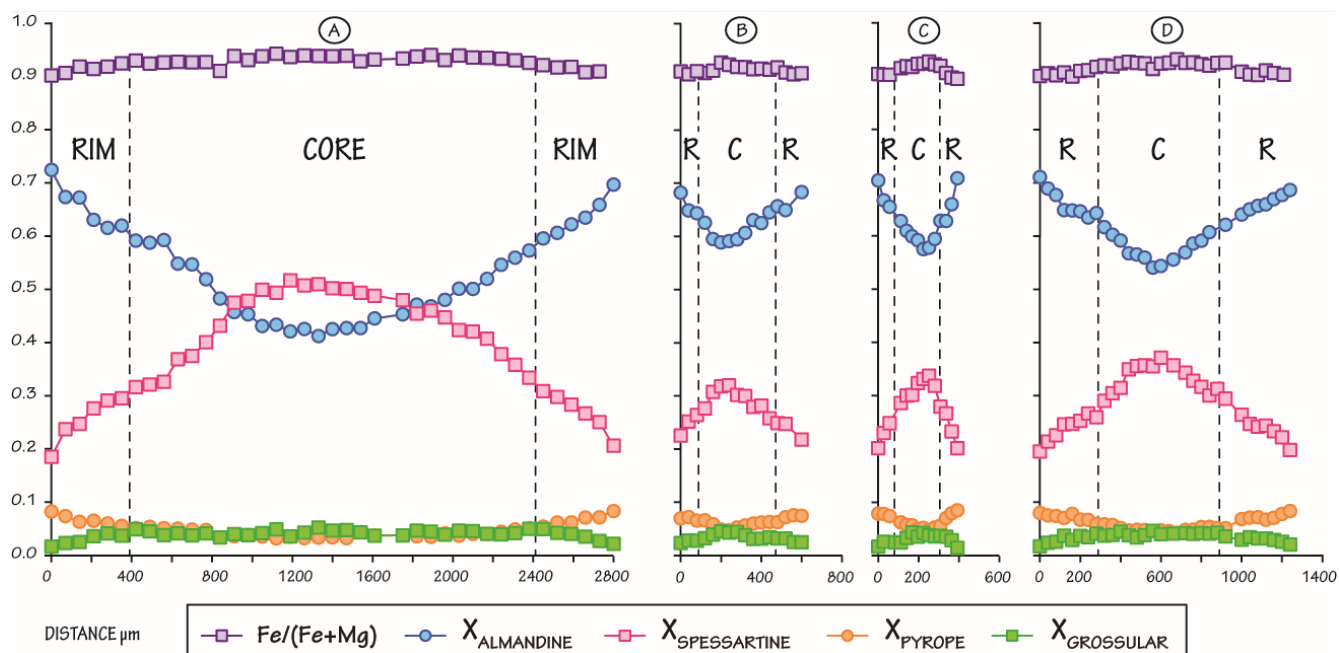
Figure 8. Garnet chemical profiles in sample MT7.
Figura 8. *Perfiles químicos de granate en la muestra MT7.*

lasts grew during prograde metamorphism (e.g. Yardley, 1977; Tracy, 1982). The decrease in grossular suggests that the growth of garnet rims may have occurred during the late prograde or early retrograde stage (e.g. Crawford, 1977; Thompson and England, 1984; Tuccillo, 1990).

Andalusite only appears in sample MT26 as sub-idiomorphic and allotriomorphic porphyroblasts (1-4 mm), which generally show an almond-like shape (Fig. 5B). They preserve a relict foliation interpreted to be S_{1-2} comprising staurolite, muscovite, biotite, chlorite, ilmenite, magnetite and quartz. Porphyroblast rims are partially replaced by biotite. Locally, they are deformed into bookshelf shaped stacked grains, twinned grains and show ondulatory extinction (Fig. 5B).

Muscovite and *biotite* appear in both samples. In MT7 two textural types are distinguished: sub-idiomorphic crystals, between 0.5 mm (muscovite) to 1.2 mm (biotite) occasionally arranged as lepidoblasts (up to 1.5 mm length) and oriented according to S_2. Locally they show wavy extinction, S/C structures and kink-bands in the most deformed domains, in which post-S_2 foliation becomes more evident. Post-S_2 micas are elongated crystals (0.5-0.8 mm in length), muscovites concentrate mainly in the tails and pressure shadows, and forming mica fish-type structures, and biotite appears associated with chlorite, partially replacing the garnet rims.

In sample MT26 three textural types of micas are distinguished: S_2 elongated sub-idiomorphic crystals (0.3-0.5 mm) included in the andalusite porphyroblasts; aggregates of lepidoblasts (0.3-1 mm) arranged in bands surrounding the andalusite porphyroblasts following the S_2 orientation and elongated crystals of between 0.4-0.6 mm in length related to post-S_2 foliation. Muscovites concentrate in the tails and pressure shadows, and biotite appears associated with chlorite, partially replacing the andalusite porphyroblasts. Si content in the S_2 muscovites show average values below 3.05 a.p.f.u. and below 3.0 a.p.f.u. in post-S_2 muscovites. Composition of all the analyzed muscovites is projected below the line of the ideal Tschermak substitution ($Al^{IV}+Al^{VI} = (Mg, Fe^{2+}) + Si^{IV}$; Fig. 9A) indicating that part of Fe^{3+} has been replaced by Al^{3+}. The projection of the proportions of Al_2O_3 *vs.* FeO_T (wt.%) in muscovites of the Riás Schists in the classification diagram for white micas proposed by Miyashiro (1973) suggests that they crystallized under "staurolite and sillimanite zone" conditions (Al_2O_3 <39.09%; FeO_T <5.07%, Fig. 9B).

Staurolite is limited to sample MT26 as sub-idiomorphic crystals (<0.4 mm) included in the andalusite porphyroblasts and idiomorphic-sub-idiomorphic crystals (<0.5 mm) scattered in the matrix (Fig. 5A). Both types show a similar Fe/(Fe+Mg) ratio in S_1=0.90 and S_2=0.92.

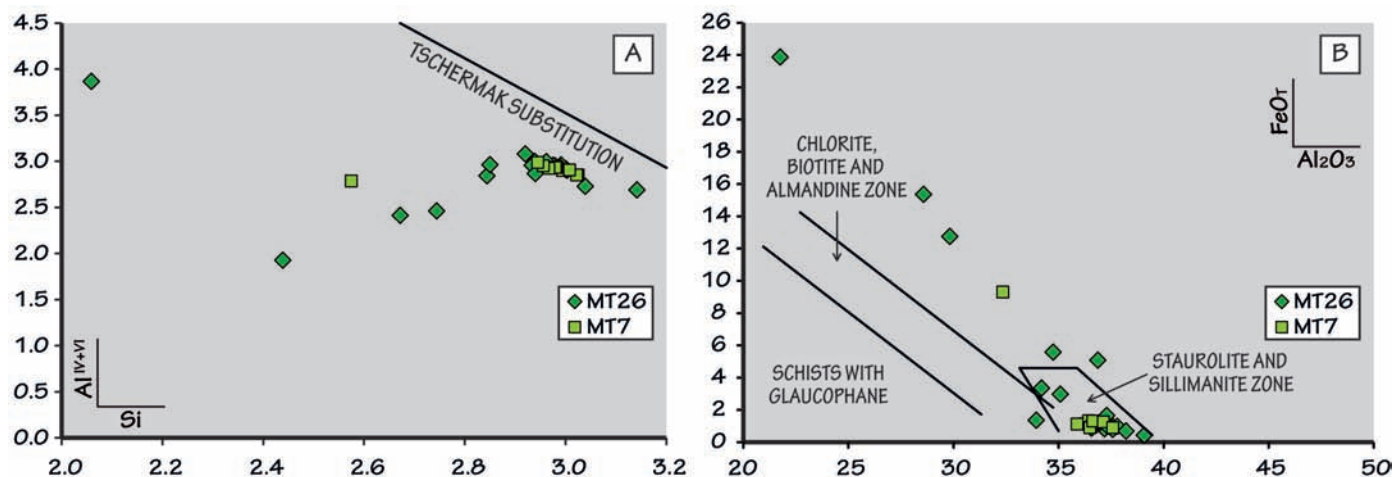*Plagioclase* in both samples is nearly pure albite

Figure 9. Electron probe microanalyses plots for white micas (A) Al^{IV+VI}–Si diagram; (B) Miyashiro s classification diagram (1973).
Figura 9. *Proyecciones de los análisis de micas blancas realizados mediante microsonda electrónica (A) Diagrama Al^{IV+VI}–Si (B) Diagrama de clasificación de micas blancas de Miyashiro (1973).*

(Ab$_{[0.98]}$An$_{[0.02]}$). Albites are sub-idiomorphic crystals (0.1 to 0.4 mm) with almond-shaped morphologies, showing simple and double twins and occasionally contain phyllosilicate micro-inclusions (<0.1 mm; Fig. 5).

Chlorite occurs in both samples. In sample MT7 S$_2$ chlorites reach up to 0.3 mm, and post-S$_2$ chlorites (0.2-0.5 mm) crystallize in the pressure shadows generated around garnet porphyroblasts. Locally, chlorite appears as a product of the alteration of muscovite and replacing the rims of garnet porphyroblasts. In sample MT26 S$_2$ chlorites reach up to 0.5 mm and post-S$_2$ chlorites are crystal aggregates (0.2-0.5 mm) located around the pressure shadows of andalusite porphyroblasts and, occasionally, as a product of the alteration of muscovite or replacing the rims of andalusite porphyroblasts associated with biotite.

The Si content in the two types of chlorites, in both samples, does not exceed 2.8 a.p.f.u., but due to its high Fe content (2.65-2.66) it is inferred that they could be classified as chamosite (Deer *et al.*, 1992). Fe/(Fe+Mg) ratio is the same in S$_2$ chlorites in both samples (X$_{Fe}$=0.99) and is slightly lower in post-S$_2$ chlorite (X$_{Fe}$=0.65).

Rutile exclusively appears as micro-inclusions (needles) in the core of garnet porphyroblasts (MT7) and as allotriomorphic crystals included in the andalusite porphyroblasts in sample MT26. In sample MT26 rutile is partially/or almost completely replaced by ilmenite. It has not been possible to identify rutile as micro-inclusions within the staurolite crystals.

Mn-rich ilmenite (2.5-5.95%) and magnetite in samples MT7 and MT26 are alotriomorphic crystals scattered in the micaceous and quartz-bearing domains that define S$_2$.

Quartz appears in both samples. In MT7 quartz micro-inclusions (<0.5 mm) are arranged parallel to the cores of the garnet porphyroblasts. Quartz sub-idiomorphic crystals of variable size (0.5-2.0 mm) are concentrated in the monomineral bands that define S$_2$ and preserve evidence of post-S$_2$ deformation (ondulatory extinction). Sub-idiomorphic crystal aggregates (0.2-0.5 mm) form the pressure tails and fill microfractures of garnet porphyroblasts. In sample MT26 quartz crystals are up to 2 mm in size and are arranged in S$_2$-bands. Crystals with wavy extinction are associated with post-S$_2$ deformation.

Tourmaline is a common accessory phase in both samples and shows intermediate compositions between schorl-dravite series leaning toward the second term. They are relatively rich in Na$_2$O (2-2.5%) and show low CaO (<0.6%) and TiO$_2$ (<1.5%) contents.

Balance of methamorphic reactions

The study of metamorphic processes requires a thorough micro-textural analysis of reaction textures. This analysis must be complemented with chemical restrictions (compositions and reaction balance) and petrological grids (projections or coherent P–T pseudo-sections) to distinguish between possible different alternatives.

The balance of metamorphic reactions solves the effect of changes in the chemical composition of a textural micro-domain in equilibrium, by solving a system of equations by linear algebra. This is applied in a pseudo-univariate system that is solved by *n* variables with *n* independent equations.

Our methodology includes the detailed study of the micro-textures and the determination of the sequence of mineral assemblages, as well as the selection of a simplified chemical system model for each reaction respecting the phase rule (K(FMMn)ASHT; K_2O-FeO-MgO-MnO-Al_2O_3-SiO_2-H_2O-TiO_2). The (stoichiometric) result of the reaction balance is additionally verified by comparing the volume ratios (observed *vs.* calculated) of the product phases (see more details in Álvarez-Valero and Kriegsman, 2010; Álvarez-Valero *et al.*, 2014).

Event M1

Petrography of this micro-domain reveals that biotite, staurolite and quartz reacted forming muscovite and garnet (core) (Table 2; Fig. 5A). This interpretation is in agreement with the results of the 5-components mass balance and volume ratio (~0.6) of the newly grown phases.

Event M2

In the second event (M2) two micro-domains were identified texturally, which are confirmed chemically by the results obtained in the mass balance calculations.

The balance of the first micro-domain (garnet-absent) matches the observations of staurolite, muscovite and quartz reacting to form biotite, andalusite and ilmenite (Table 3A; Fig. 5B). The second micro-domain shows that biotite, staurolite, garnet (core) and quartz react to form muscovite, garnet (rim), chlo-rite and ilmenite (Table 3B; Fig. 5B). Both micro-domains are coherent with the calculated volume ratios (~0.4 and ~0.91, respectively).

Thermobarometry: *P T Pseudo-sections*

P–T pseudo-sections allow us to model natural systems (i.e. representative micro-domains) using an effective composition for a particular rock (Table 4). P–T diagrams for both samples have been calculated between 400 and 650 °C and 0-1.0 GPa in the chemical system MnNCKFMASHTO, assuming H_2O in excess, using Theriak-Domino (v. 04.02.2017; de Capitani and Brown, 1987) and the internally consistent thermodynamic dataset of Holland and Powell (2011).

References for the mixing models for solid solutions of the phases considered in the calculations are biotite (White *et al.*, 2014a,b), chloritoid (Holland and Powell, 2011; White *et al.*, 2014a), chlorite (Holland and Powell, 2011; Powell *et al.*, 2014), cordierite (Holland and Powell, 2011; White *et al.*, 2014a,b), epidote (Holland and Powell, 2011), garnet (White *et al.*, 2014a,b), ilmenite (White *et al.*, 2000), magnetite (White *et al.*, 2000), plagioclase (Holland and Powell, 2003), staurolite (Holland and Powell, 2011; White *et al.*, 2014a), and white mica (Smye *et al.*, 2010; Holland and Powell,, 2011; White *et al.*, 2014b). Andalusite-sillimanite-kyanite-pyrophillite, lawsonite, rutile, quartz and albite were considered pure phases (activity = 1).

In these samples there is no a significant amount of chemical zoning in minerals. Therfore, bulk rock compositions determined by X-ray fluorescence analysis are interpreted as the reactive bulk rock compositions (e.g. Lanari and Engi, 2017) resulting from

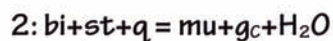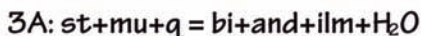| Sample	MT26	MT26	MT26	MT7		
Analysis	22	13	19	60		
Phase	bi	st	mu	g (core)	q	H_2O
$KO_{0.5}$	0.96	0.00	0.86	0.00	0.00	0.00
$(Fe,Mg,Mn)O$	2.14	2.56	0.10	2.84	0.00	0.00
$AlO_{1.5}$	2.00	18.75	2.93	2.06	0.00	0.00
SiO_2	2.56	7.46	3.10	2.93	1.00	0.00
H_2O	1.00	2.00	1.00	0.00	0.00	1.00
Reaction Coefficients	4.814	0.780	-5.374	-4.147	10.622	-1.000

$$2: bi+st+q = mu+g_c+H_2O$$

Table 2. Chemical composition of the phases used to calculate the balance of metamorphic reactions in the K(FMMn)ASH chemical system for Stage M_1.
Tabla 2. *Composición química de las fases empleadas en los cálculos de balance de reacciones metamórficas en el sistema químico K(FMMn)ASH para el Evento M_1*

Sample	MT26	MT26	MT26	MT26		MT7	
Analysis	224	213	223	21		202	
Phase	bi	st	mu	and	q	ilm	H_2O
$KO_{0.5}$	0.92	0.00	0.82	0.00	0.00	0.00	0.00
$(Fe.Mg.Mn)O$	2.15	2.62	0.33	0.01	0.00	0.95	0.00
$AlO_{1.5}$	2.00	18.88	2.93	2.05	0.00	0.01	0.00
SiO_2	2.57	7.39	2.85	0.96	1.00	0.00	0.00
TiO_2	0.11	0.13	0.02	0.00	0.00	1.02	0.00
H_2O	1.00	2.00	1.00	0.00	0.00	0.00	1.00
Reaction Coefficients	-0.650	0.460	0.729	-4.648	0.652	-0.003	-1.000

3A: st+mu+q = bi+and+ilm+H_2O

Sample	MT26	MT26	MT7		MT26	MT26	MT7		MT7
Analysis	224	13	86		223	217	202		81
Phase	bi	st	g (core)	q	mu	chl	ilm	H_2O	g (rim)
SiO_2	2.57	7.46	2.93	1.00	3.00	2.50	0.00	0.00	2.85
$AlO_{1.5}$	1.96	18.75	2.08	0.00	2.90	3.15	0.00	0.00	2.22
FeO	1.48	2.25	1.60	0.00	0.06	2.76	0.83	0.00	1.89
MgO	0.78	0.18	0.11	0.00	0.07	1.45	0.00	0.00	0.18
MnO	0.01	0.13	1.19	0.00	0.00	0.03	1.02	0.00	0.76
$KO_{0.5}$	0.89	0.00	0.00	0.00	0.87	0.01	0.00	0.00	0.01
TiO_2	0.07	0.10	0.18	0.00	0.01	0.01	1.02	0.00	0.00
H_2O	2.00	2.00	0.00	0.00	1.00	2.00	0.00	1.00	0.00
Reaction Coefficients	1.723	0.251	0.843	1.340	-1.743	-0.816	-0.263	-0.312	-1.000

3B: bi+st+g_C+q = mu+g_R+chl+ilm+H_2O

Table 3. Chemical composition of the phases used to calculate the balance of metamorphic reactions for Stage M_2 in (A) a six-component K(FMMn)ASHTi chemical system, and (B) 8-components KFMMnASHTi chemical system.
Tabla 3. Composición química de las fases empleadas en los cálculos de balance de reacciones metamórficas para el Evento M2 en (A) un sistema químico de 6 componentes K(FMMn)ASHTi, y (B) de 8 componentes KFMMnASHTi.

Oxide	wt % (Actlabs)		mole % atoms MnNCKFMASHTO	
	MT7	MT26	MT7	MT26
SiO_2	46.59	67.53	45.96	67.00
TiO_2	1.06	0.73	0.79	0.54
Al_2O_3	26.34	17.51	30.64	20.48
FeO	7.50	4.60	6.19	3.82
MnO	0.17	0.053	0.14	0.04
MgO	2.96	1.19	4.35	1.76
CaO	0.13	0.06	0.14	0.06
Na_2O	0.74	0.35	1.42	0.67
K_2O	7.51	4.06	9.45	5.14
Fe_2O_3	1.25	0.64	0.93	0.48

Table 4. Bulk-rock compositions for samples MT7 and MT26.
Tabla 4. Composición de roca total de las muestras MT7 y MT26.

the reacting set of minerals and fluid/s at, or immediately after, the metamorphic peak, after garnet removed significant amounts of Mn, Ca, Mg and Fe, thus modifying the effective bulk composition of the rocks.

The estimated values for sample MT7 (Fig. 10) suggests decompression from 0.6 to 0.3 GPa, with moderate cooling (580–550 °C), from the garnet-bearing field g+mu+bi+st+chl+mt+ilm+q (M_2) to the and-bearing field with stable plagioclase, pl+g+mu+bi+chl+mt+ilm+and+q (post-M_2). Accurate P–T conditions for M_2 (0.6 GPa, 580 °C) and post-M_2 (0.3 GPa, 550 °C) have been deduced based on the intersection between the silica content in muscovite isopleths (Si(mu) <3.05 for M_2; Si(mu)<3.0 for post-M_2) and garnet rim isopleths (X_{Mn}=0.25-0.2; X_{Ca} <0.1).

For sample MT26 (Fig. 11) the estimated values suggest decompression from 0. 5 to 0.3 GPa, with a decrease in temperature from 570 to 540 °C, from the garnet-out field mu+bi+st+chl+mt+ilm+q (M_2) to the
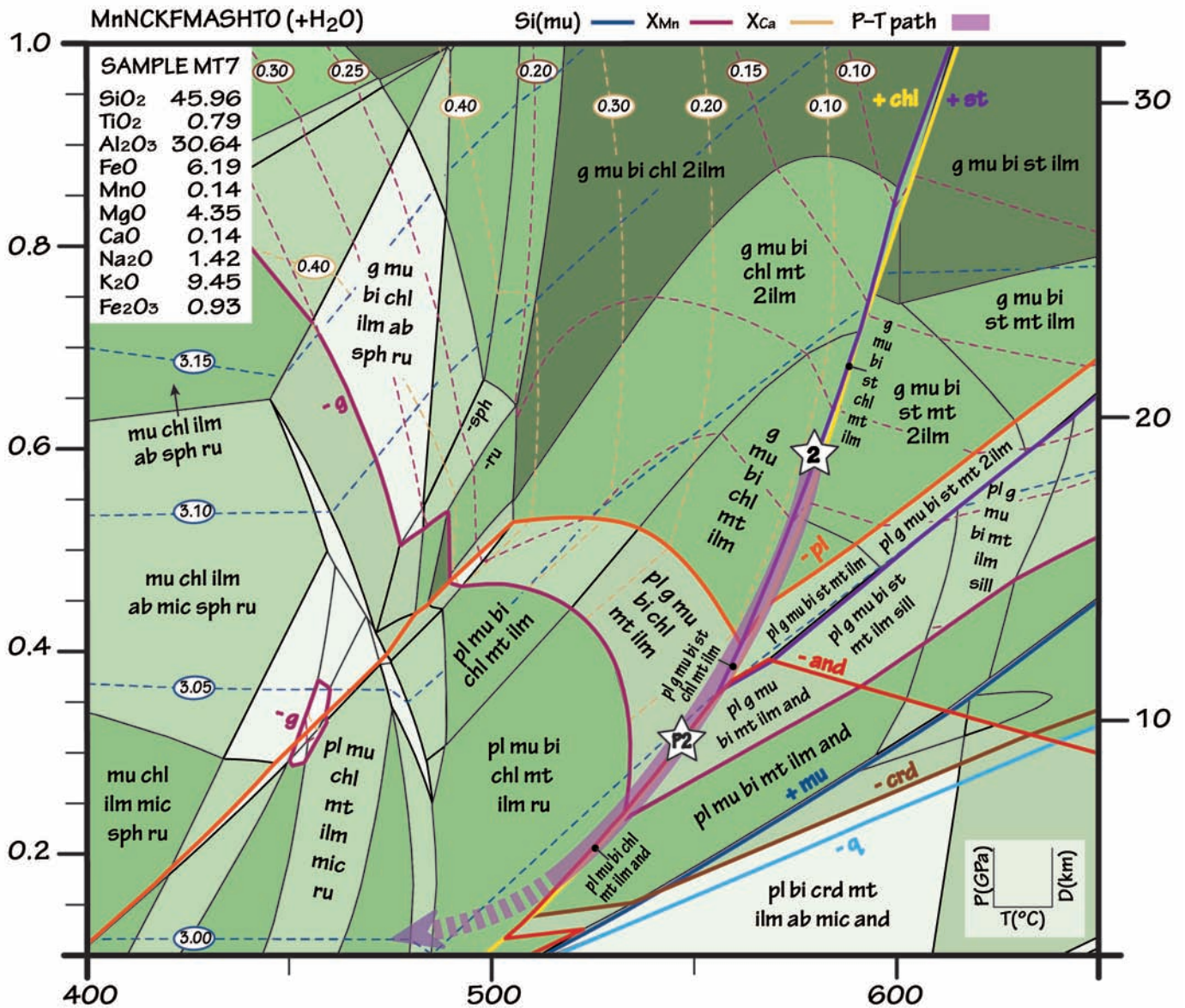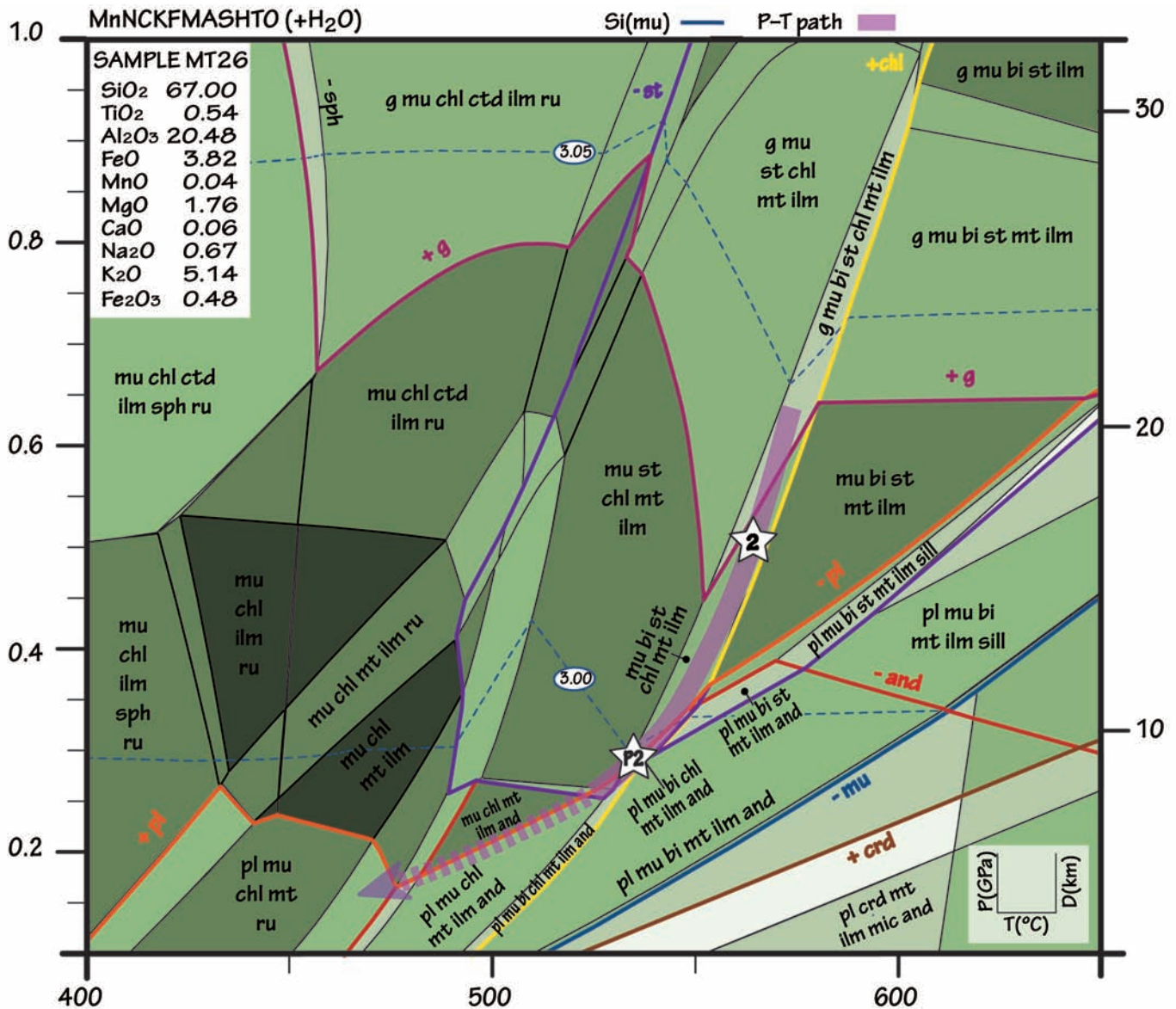
Figure 10. P–T pseudo-section calculated for the garnet-bearing micaschist (MT7).
Figura 10. Pseudosección P–T calculada para el micaesquisto con granate (MT7).

field pl+mu+bi+chl+mt+ilm+and+q (post-M₂). The minimum pressure for M₂ has been estimated based on the silica content in muscovite isopleths (Si(mu) <3.05). The calculated model predicts that the stability fields of garnet and andalusite do not coexist, as observed at outcrop and thin section scales.

Discussion

(1) P–T Conditions:
    The results obtained from P–T pseudo-sections

(Figs. 10 and 11) agree with the natural observations in the studied thin sections.
    In the case that both studied lithologies experienced the same structural and metamorphic evolution, and therefore, the growth or absence of certain phases is determined by their bulk rock chemistry, based on textural observations, three correlatable foliations can been identified in the Riás Schists: S₁, preserved in the core of garnet porphyroblasts and staurolite crystals; the matrix foliation S₂, that includes the garnet porphyroblasts rims, staurolite, muscovite, biotite, rutile/ilmenite, magnetite, chlorite

Figure 11. P–T pseudo-section calculated for the andalusite-bearing micaschist (MT26).
Figura 11. Pseudosección P–Tcalculada para el micaesquisto con andalucita (MT26).

and quartz, together with the development of syntectonic andalusite; and post-S$_2$ that comprises andalusite and albitic plagioclase and secondary muscovite, biotite, chlorite, quartz and accessory tourmaline, Fe/Ti oxides, apatite and carbonate.

Multiequilibrium termobarometry using P–T pseudosections suggests that M$_2$ represents the metamorphic peak, the deepest burial depth, and it has been estimated at minimum pressures of *ca.* 0.6 GPa and 580 °C in garnet-micaschists (Sample MT7), which would be equivalent to *ca.* 20 km burial depth. The retrograde stage records decompression from the kyanite stability zone in the amphibolite facies, to the

andalusite stability zone in the greenschist facies. Peak metamorphic conditions for M$_2$ in andalusite-bearing micaschists suggest very similar values, minimum pressures of *ca.* 0.5 GPa and 570 °C (Fig. 12).

The complexity involved in subtracting zoned garnet, or andalusite porphyroblasts, from the bulk rock composition analysed by X-ray fluorescence, to calculate different effective or reactive compositions for each metamorphic event, exceeded the objectives of the research carried out for this study. For this reason, the M$_1$ event has not been quantified and the pressure and temperature values obtained for M$_2$ and Post-M$_2$ may be underestimated. It is therefore necessary to
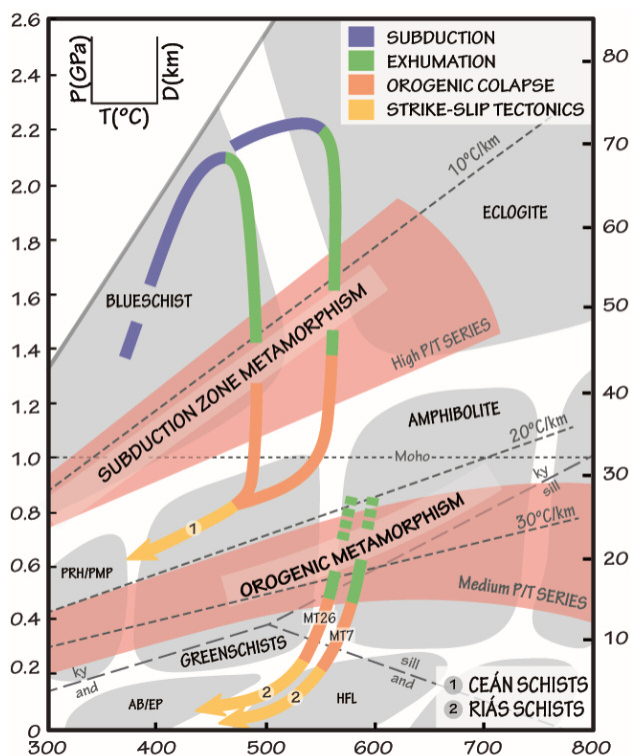
Figure 12. P–T diagram showing a summary of the P–T paths of the Ceán Schists (López-Carmona *et al.*, 2013; 2014) and the Riás Schists (this study). The main metamorphic facies, facies series and the corresponding tectonic environment are also shown as reference (modified from Miyashiro, 1961; Yardley, 1989). PRH/PMP: prehnite-pumpellyite; AB/EP: albite-epidote; HFL: hornfels.

Figura 12. Diagrama P–T que muestra un resumen de las trayectorias P–T de los Esquistos de Ceán (López-Carmona et al., 2013; 2014) y de los Esquistos de Riás. Las facies metamórficas principales, las series de facies y los ambientes tectónicos asociados se incluyen como referencia (modificado de Miyashiro, 1961; Yardley, 1989). PRH/PMP: prehnita-pumpellita; AB/EP: albita-epidota; HFL: corneana.

investigate more deeply these aspects in order to better understand this terrain evolution.

On the other hand, if each of the lithological types described reflects a different structural position in the original pile and therefore, recorded different metamorphic conditions, garnet and andalusite never coexisted in equilibrium in the same paragenesis. Thus, in the structurally upper sequence (to the W; sample MT7) garnet- and staurolite-Barrovian zones may be distinguished, whereas the structurally lower sequence (to the E; sample MT26) may be characterized by a high-temperature/low-pressure Buchan-type metamorphism in the andalusite zone.

Given the disposition of these lithologies in the studied outcrop, and their proximity, this would imply justifying such an important condensation of the original pile and the presence of a major tectonic detach-

ment, which, to the best of our knowledge, is not the case.

(2) Ceán Schists vs. Riás Schists:

Contrasting metamorphism in adjacent terranes is distinctive of large-scale tectonic events that include both collision and rifting scenarios. When one of those terranes is characterized by the presence of high-pressure rocks, it is more likely to be related to collision settings, and commonly in locations close to the suture.

The Ceán Schists outcrop in the MTC, to the west of the study area. These schists represent the westernmost margin of Gondwana subducted during the Variscan orogeny (in Devonian times). They experienced a metamorphic evolution in the blueschist-facies conditions, reaching *ca*. 70 km deep ($P_{max} \sim 2.2$ GPa, López-Carmona *et al*., 2013). Estimations made in the Riás Schists, and the spatial relationship between both lithologies (see Figs. 2 and 3) suggest that they formed part of the same continental margin at the beginning of the Variscan orogeny, but experienced very different tectonothermal evolutions due to their putative position in the passive margin and hence, in the orogenic wedge (Fig. 12).

The projection of the proportions of Al_2O_3 vs. FeO_T (wt. %) in Miyashiro's diagram for white mica classification (1973; Fig. 9B) allows the visualization of the relationships among three representative lithologies of the allochthon (Ceán Schists), parautochthon (Riás Schists) and autochthon (gneisses and micaschists of Viana do Bolo; Díez Montes, 2007). From the diagram, it can be deduced that the Riás Schists ($Al_2O_3 < 39.09\%$; $FeO_T < 5.07\%$; staurolite and sillimanite zones) and the Ceán Schists ($Al_2O_3 < 30.27\%$; $FeO_T < 4.62\%$; schists with glaucophane; López-Carmona *et al*., 2007) experienced significantly different metamorphic evolutions. In contrast, micas from the Viana do Bolo Serie ($Al_2O_3 < 36.9\%$, $FeO_T < 1.09\%$; Díez Montes, 2007) are also projected in the staurolite and sillimanite zones, suggesting that white mica crystallization conditions were similar to those of the Riás Schists (Fig. 13).

The Lower Allochthon recorded the continental subduction event (blueschist- and eclogite-facies conditions) of the most external part of the north Gondwana passive margin during the late Devonian (*ca*. 370-365 Ma) at the beginning of the Variscan collision (López-Carmona *et al*., 2014), followed by a buoyancy-driven exhumation triggered by the extensional collapse of the orogenic pile. Contrarily, the underlying parauthochthon underwent crustal thickening, resulting in a medium-pressure Barrovian-type metamorphism and possibly, was followed by a higher temperature/lower pressure Buchan-type metamorphism that could be related to tectonic exhuma-

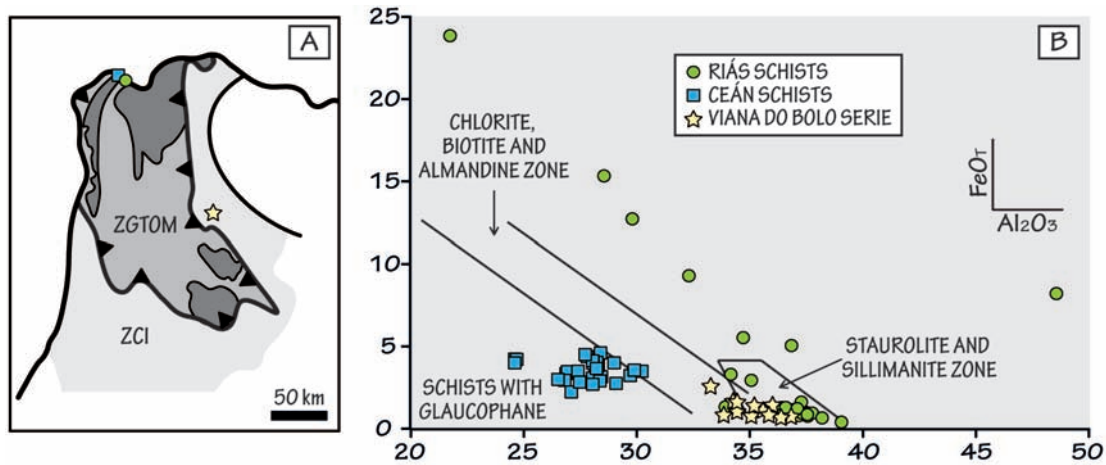**Figure 13.** (A) Location of the samples used for comparison in this study; (B) Miyashiro s white micas classification diagram (1973) for the Riás Schists, the Ceán Schists (López-Carmona, 2007) and the Viana do Bolo Serie (Díez-Montes, 2007).
Figura 13. (A) Ubicación de las muestras usadas para realizar la comparación en este trabajo; (B) Diagrama de clasificación de micas blancas de Miyashiro (1973) para los Esquistos de Riás, los Esquistos de Ceán (López-Carmona, 2007) y la Serie Viana do Bolo (Díez-Montes, 2007).

tion and/or erosion (e.g. Gutiérrez-Alonso *et al.*, 2018). Furthermore, the authocthon (CIZ) recorded similar metamorphism to that of the parautochthon (e.g. Martínez Catalán *et al.*, 2014). Figure 14 shows a summary of the relationships between deformation phases (D) and metamorphic events (M) in representative units of the autochthon (CIZ), parautochthon (this study) and the allochthon (MTC) of the GTOMZ.

Conclusions

Three metamorphic events have been identified in the Riás Schists: (i) M$_1$, preserved in the core of garnet

and staurolite crystals; (ii) M$_2$, which comprises the matrix foliation, S$_2$, and the paragenesis g$_{RIM}$ + st + mu + bi + ilm + mt + chl + q together with syntectonic andalusite; and (iii) Post-M2 (post-S$_2$) including and + pl + mu + bi + chl + q ± tourmaline, Fe /Ti, oxides and carbonate.

Thermobarometric estimations, integrated within a comprehensive petrological study, suggest that the Riás Schists experienced a medium-pressure Barrovian metamorphic evolution.

Multi-equilibrium termobarometry using pseudo-sections yields minimum P–T values of 0.5-0.6 GPa, 580-570 °C for M$_2$ and 0.3 GPa, 540 °C for post-M$_2$. The calculated model for the andalusite-bearing micas-

Figure 14. Comparative chart depicting the deformation phases (D) and metamorphic stages (M) in the Malpica-Tui Complex (Diéz Fernández *et al.*, 2012; López-Carmona *et al.*, 2013; 2014), in the Schistose Domain (this study) and in the Central Iberian Zone (Martínez-Catalán *et al.*, 2014).
Figura 14. Cuadro comparativo en el que se muestran las fases de deformación (D) y los estadios metamórficos (M) en el Complejo de Malpica-Tui (Diéz-Fernández et al., 2012; López-Carmona et al., 2013; 2014), el Dominio Esquistoso (este trabajo) y la Zona Centroibérica (Martínez-Catalán et al., 2014).

chists (sample MT7) also predicts that the stability fields of garnet and andalusite, for the reactive bulk rock composition used, do not coexist, as observed at outcrop and thin section scales.

The pelitic schists from the parauthochthon (i.e. Riás Schists) and the pelitic schists from the MTC (i.e. Ceán Schists) experienced very different tectonothermal evolutions despite their proximity in their current geographic location.

Acknowledgements

References

Abati, J. 2000. Petrología Metamórfica y Geocronología de la unidad culminante del Complejo de Órdenes en la región de Carballo (Galicia, NW del Macizo Ibérico). *Serie Nova Terra*, 20. 269 pp. Alonso, J.L. and González, J.C., 1982. Mapa Geológico Nacional Sisargas-Carballo. Instituto Geológico y Minero de España, Hoja 44, Escala 1:50.000.

Álvarez-Valero, A. and Kriegsman, L. 2010. Chemical, petrological and mass balance constraints on the textural evolution of pelitic enclaves. *Lithos,* 116, 300–309.

Álvarez-Valero, A., Gómez-Barreiro, J., Alampi, A., Castiñeiras, P. and Martínez-Catalán, J. 2014. Local isobaric heating above an extensional detachment in the middle crust of a Variscan allochthonous terrane (Órdenes complex, NW Spain). *Lithosphere,* 6, 409–418.

Arenas, R. 1988. Evolución petrológica y geoquímica de la unidad alóctona inferior del complejo metamórfico básico-ultrabásico de Cano Ortegal (Unidad de Moeche) y del Silúrico paraauctóctono, Cadena Hercínica Ibérica (NW de España). *Corpus Geologicum Gallaeciae*, 4, 543 pp.

Arenas, R., Sánchez Martínez, S., Díez-Fernández, R., Gerdes, A., Abati, J., Fernández- Suárez J., Andonaegui, P., González Cuadra, P., López Carmona, A., Richard A., Fuenlabrada, J. and Rubio Pascual, J. 2016. Allocthonous terranes involved in the Variscan suture of

NW Iberia: A review of their origin and tectonothermal evolution. *Earth- Science Reviews,* 161, 140–178.

Atherton, M. 1968. The variation in the garnet, biotite and chlorite composition in médium grade pelitic rocks from Dalradian, Scotland with particular reference to the zonation in garnet. *Contribution to Mineralogy and Petrology*, 18, 347–371.

Atherton, M. and Brotherton, M. 1982. Major element composition of the pelites of the Scottish Dalradian. *Geological Journal*, 17, 185–221.

Ballèvre, M., Martínez Catalán, J., López-Carmona, A., Pitra, P., Abati, J., Díez-Fernández, R., Ducassou, C., Arena, R., Bosse, V., Castiñeiras, P, Fernández-Suárez, J., Gómez Barreiro, J., Paquette, J., Peacut, J., Poujol, M., Ruffet, G. and Sánchez Martínez, S. 2014. Correlation of the nappe stack in the Ibero-Armonican arc across the Bay of Biscay: a joint French-Spanish Project. *Geological Society, London, Special Publications*, 405. Lyell Colletion. London – England, 38.

Barrow, G. 1893. On an intrusión of muscovite-biotite gneiss in the southeastern Highlands of Scotland and its accompanying metamorphism. *Quarterly Journal of the Geological Society of London*, 49 (3), 87–93.

Bucher, K. and Grapes, R. 2011. *Metamorphism of Pelitic (Metapelites).* In: Petrogenesis of Metamorphic Rocks, DOI 10.1007/978-3-540-74169-5_7, Springer-Verlag Berlin Heidelberg, 257–313.

Coke, C. and Ribeiro, A. 2000. Malpica–Lamego shear zone; A major crustal discontinuity in the Iberian Variscan fold belt, Program and Abstracts – *International Conference on Basement Tectonics*, 15, 208–210.

Connolly, J. and Petrini, K. 2002. An automated strategy for calculation of phase diagram sections and retrieval of rock properties as a function of physical conditions. *Journal of Metamorphics Geology*, 20, 697–708.

Crawford, M.L. 1977, Calcium zoning in almandine garnet, Wissahickon Formation, Philadelphia, Pennsylvania. *Canadian Mineralogist*, 15, 243–249.

Dallmeyer, R., Martínez Catalán, J., Arenas, R., Gil Ibarguchi J., Gutiérrez Alonso, G., Farias, P., Aller, J. and Bastida, F. 1997. Diachronous Variscan tectonothermal activity in the NW Iberian Massif: Evidence from $^{40}Ar/^{39}Ar$ dating of regional fabrics. *Tectonophysics,* 277, 307–337.

De Capitani C. and Brown T.H. 1987. The computation of chemical equilibrium in complex systems containing non–ideal solutions. *Geochimica et Cosmochimica Acta*, 52, 639–652.

Deer, W., Howie, R. y Zussman, J. 1992. *An Introduction to the Rock-Forming Minerals*. Second Edition. Longman Scientific & Technical. London – England, 687 pp.

Dias da Silva, I., Valverde–Vaquero, P., González Clavijo, E., Díez Montes. A. and Martínez Catalán, J. 2012. Structural and stratigraphical significance of U/Pb ages from the Saldanha and Mora volcanic complexes (NE Portugal, Iberian Variscides). In: Length scales, times scales and relative contribution of Variscan orogenic events to formation of European crust. Geologie de la France 2012–1, 105 – 106.

Díaz García, F. 1992. Propuesta de una nueva zona en el Hercínico de la Península Ibérica. *Cuadernos do Lab. Xeolóxico de Laxe*, 17, 199–207.

Díez Montes, A. 2007. Geología del Dominio "Ollo de Sapo" en las comarcas de Sanabria y Terra do Bolo. *Serie Nova Terra,* 34, 414 pp.

Díez Fernández, R. 2011. Evolución estructural y cinemática de una corteza continental subducida: La Unidad de Malpica-Tui (NO del Macizo Ibérico). *Serie Nova Terra*, 40, 228 pp.

Díez Fernández, R., Martínez Catalán, J., Arenas, R. and Abati, J. 2011. Tectonic evolution of a continental sub-duction-exhumation channel: Variscan structure of the basal allocthonous units in NW Spain. Tectonics. Vol. 30, American Geophysical Union – TC3009.

Díez Fernández, R., Martínez Catalán, J., Gómez-Barreiro, J. and Arenas, R. 2012. Extensional flow during gravitational collapse: a tool for setting plate convergence (Padrón migmatitic dome, Variscan belt, NW Iberia). *Journal of Geology*, 120, 83–103.

Evans, T. 2004a. A method for calculating effective bulk composition modification due to crystal fractionation in garnet-bearing schists: implications for isopleth termo-barometry. *Journal of Metamorphic Geology*, 22, 547–557.

Evans, T. 2004b. Reconciling the structural and metamorphic record of orogeny in central western New Hampshire through microstructure and garnet isopleth termobarometry. Unpublished PhD Thesis, James Cook University, 89 pp.

Farias, P., Gallastegui, G., González-Lodeiro, F. Marquínez, J. Martín Parra, L., Martínez Catalán, J., Pablo Maciá, J. y Rodríguez Fernández, L. 1987. Aportaciones al conocimiento de la litoestratigrafía y estructura de Galicia Central. Memórias da Faculdade de Ciências, Universidade do Porto, 1, 411–431.

Gil Ibarguchi, J. and Ortega Gironés, E. 1985. Petrology, structure and geotectonic implications of glaucophane–bearing eclogites and related rocks from the Malpica–Tuy unit, Galicia, northwest Spain. *Chemical Geology*, 50, 145–162.

Gómez Barreiro, J., Martínez Catalán, J., Arenas, R., Castiñeiras, P., Abati, J., Díaz García, F. and Kraft, R. 2007. Tectonic evolution of the upper allochthon of the Órdenes complex (northwestern Iberian Massif): Structural constraints to a polyorogenic peri-Gondwanan terrane. *Geological Society of America*, 423, 315–322.

Gómez, J. 2006. Metamorfismo. Apuntes de la asignatura Petrología Endógena II (Módulo I). Tercer curso de la Licenciatura de Geología – Departamento de Ciencias de la Tierra. Universidad de Zaragoza – España, 199 pp.

Gutiérrez-Alonso, G., Collins, A. S., Fernández-Suárez, J., Pastor-Galán, D., González-Clavijo, E., Jourdan, F., Weil, A.B. and Johnston, S. T. 2015. Dating of lithospheric buckling: 40Ar/39Ar ages of syn-orocline strike–slip shear zones in northwestern Iberia. *Tectonophysics*, 643, 44–54.

Gutiérrez-Alonso, G., Fernández-Suárez, J., López-Carmona, A., and Gärtner, A. 2018. Exhuming a cold case: The early granodiorites of the northwest Iberian Variscan belt—A Visean magmatic flare-up?. *Lithosphere*, 10(2), 194-216.

Hey, M. 1954. A new rewiev of the chlorites. *Mineralogical Magazine*, 30, 277–292.

Holland T. and Powell, R. 2000. In: Powell, R. and Holland T. (2002). Course Notes for THERMOCALC Workshop 2002: Calculating Metamorphic Phase Equilibria (Barcelona). CD–ROM.

Holland, T. J. B. and Powell, R. 2011. An improved and extended internally consistent thermodynamic dataset for phases of petrological interest, involving a new equation of state for solids. Journal of Metamorphic Geology, 29, 333–383. Holland, T. J. B. and Powell, R. 2003. Activity-composition relations for phases in petrological calculations: an asymmetric multicomponent formulation. *Contributions to Mineralogy and Petrology*, 145, 492–501.

Hollister, L. 1966. Garnet zoning: an interpretation based on the Rayleigh fractionation model. *Science*, 154, 1647–1651.

Julivert, M., Fontoté, J., Ribeiro, A. and Conde, L. 1972. Mapa Tectónico de la Península Ibérica y Baleares, E 1:1.000.000. Instituto Geológico y Minero de España, Madrid.

Julivert, M., Fontoté, J., Ribeiro, A. and Conde, L. 1980. Mapa Tectónico de la Península Ibérica y Baleares, E 1:1.000.000 y Memoria explicativa. Instituto Geológico y Minero de España, Madrid, 113 pp.

Lanari, P and Engi, M. 2017. Local Bulk Composition Effects on Metamorphic Mineral Assemblages. *Reviews in Mineralogy & Geochemistry*, 83, 55–102.

Li, B. and Massonne, H.J., 2016. Early Variscan P-T evolution of an eclogite body and adjacent orthogneiss from the northern Malpica-Tuy shear-zone in NW Spain. *European Journal of Mineralogy*, 28, 1131-1154.

Llana-Fúnez, S. 2011. La estructura de la unidad Malpica-Tui (Cordillera varisca en Iberia). Series de Tesis Doctorales 1. Madrid, Instituto Geológico y Minero de España (IGME), 163 pp.

López-Carmona, A. 2007. Evolución Metamórfica de los Esquistos de Ceán, Unidad de Malpica – Tui (NW del Macizo Ibérico). MSc Thesis – Universidad Complutense de Madrid. España, 99 pp.

López-Carmona, A. 2015. Blueschist-facies rocks from the Malpica-Tui Complex (NW Iberian Massif). *Serie Nova Terra*, 47, A Coruña – España, 299 pp.

López-Carmona, A., Abati, J. and Reche, J. 2007. Phase equilibrium modelling in the KFAMSH system to show the metamorphic Evolution of the Ceán Schists (Malpica-Tui Unit, NW Iberian Massif). *Geogaceta*, 44, 27–30.

López-Carmona, A., Abati, J. and Reche, J. 2010. Petrologic modeling of chloritoid–glaucophane schists from the NW Iberian Massif. *Gondwana Research*, 17, 377–391.

López-Carmona, A., Abati, J., Pitra, P. and Lee, J. 2014. Retrogressed lawsonite blueschists from the NW Iberian Massif: P–T–t constraints from thermodynamic modelling and 40Ar/39Ar geochronology. DOI 10.1007/s00410-014-0987-5. *Contributions Mineral Petrology*, 167–987.

López–Carmona, A., Pitra, P. and Abati, J. 2013. Blueschist–facies metapelites from the Malpica–Tui Unit (NW Iberian Massif): phase equilibria modelling and H₂O

and Fe$_2$O$_3$ influence in high–pressure assembalges. *Journal of Metamorphic Geology,* 31, 263–280.

Marquínez-García, J. 1984. La geología del área esquistosa de Galicia Central (Cordillera Herciniana, NW de España). Memorias del Instituto Geológico y Minero de España (IGME) 100, 231 pp.

Martínez Catalán, J.R., Arenas, R., Abati, J., Sánchez Martínez, S., Díaz García, F., Fernández Suárez, J., González Cuadra, P., Castiñeiras, P., Gómez Barreiro, J., Díez Montes, A., González Clavijo, E., Rubio Pascual, F., Andonaegui, P., Jeffries, T., Alcock, J., Díez-Fernández, R. and López-Carmona, A. 2009. A rootless suture and the loss of the roots of a mountain chain: the Variscan belt of NW Iberia. *Comptes Rendus Geoscience*, 341, 114–126.

Martínez Catalán, J.R., Arenas, R., Díaz García, F., Gómez Barreiro, J., González Cuadra, P., Abati, J., Castiñeiras, P., Fernández Suárez, J., Sánchez Martínez, S., Andonaegui, P., González Clavijo, E., Díez Montes, A., Rubio Pascal, F. and Valle Aguado, B. 2007. Space and time in time in the tectonic evolution of the northwestern Iberian Massif. Implications for the comprehension of the Variscan belt. *Geological Society of America Memoir*, 200, USA. 403–423.

Martínez Catalán, J.R., Díaz García, F., Arenas, R., Abati, J., Castineiras, P., González Cuadra, P., Gómez Barreiro, J. and Rubio Pascual, F. 2002. Thrust and detachment system in Ordenes Complex (northwestern Spain): Implications for the Variscan–Appalachian Dynamics: the Building of the late Paleozoic Basement. *Geological Society of America Special Paper* 364, 163–182.

Martínez Catalán, J.R., Rubio-Pascual, F.J., Díez Montes, A., Díez-Fernández, R., Gómez-Barreiro, J., Días da Silva, I., González Clavijo, E., Ayarza, P. and Alcock, J.E. 2014. The late Variscan HT/LP metamorphic event in NW and Central Iberia: relationships to crustal thickening, extension, orocline development and crustal evolution. In: The Variscan Orogeny: Extent, Timescale and the Formation of the European Crust. (Schulmann *et al.*, Eds.). Geological Society, London, Special Publications, 405, http://dx.doi.org/10.1144/SP405.1

Miyashiro, A. 1973. Metamorphism and metamorphic belts – 1ª Edición. G. Allen and Unwin Publications, London – England, 492 pp.

Murphy, J. B., and Gutiérrez-Alonso, G. 2008. The origin of the Variscan upper allochthons in the Ortegal Complex, northwestern Iberia: Sm–Nd isotopic constraints on the closure of the Rheic Ocean. *Canadian Journal of Earth Sciences*, 45(6), 651–668.

Powell, R and Holland, T. 1988. An internally consistent dataset with uncertainties and correlations: 3. Applications to geobarometry, worked examples and a computer program. *Journal of Metamorphic Geology*, 6, 173–204.

Powell, R. and Holland, T. 1994. Optimal geothermometry and geobarometry. *American Mineralogist*, 79, 120–133.

Powell, R., White, R.W., Green, E.C.R., Holland, T.J.B. and Diener, J.F.A. 2014. On parameterising thermodynamic descriptions of minerals for petrological calculations. *Journal of Metamorphic Geology*, 32, 245–260.

Puelles, P., Ábalos, B., Gil Ibarguchi, J. and Rodríguez, J. 2017. Scales of deformation partitioning during exhumation in a continental subduction channel: A petrofabric study of eclogites and gneisses from NW Spain (Malpica Tui Allochthonous Complex). *Journal of Metamorphic Geology*, 36, 225–254.

Ribeiro, A., Pereira, E. and Dias, R. 1990. Structure in the Northwest of the Iberian Peninsula. In: Dallmeyer, R.D. and Martinez Garcia, E. (eds). Pre–Mesozoic geology of Iberia. Springer–Verlag, Heidelberg, 220–236

Ries, A. and Shackleton, R. 1971. Catazonal complexes of North–West Spain and North Portugal, remnants of a Hercynian thrust plate. *Nature*, 234, 65–69.

Rodríguez, J. 2005. Recristalización y deformación de litologías supracorticales sometidas a metamorfismo de alta presión (Complejo de Malpica–Tui, NO del Macizo Iberico). *Nova Terra,* 29, 410 pp.

Rubio Pascual, F. 1991. Metamorfismo de alta presión y superposición de un gradiente metamórfico invertido en los esquistos de la Unidad de Santiago (Complejo de Órdenes, Zona de Galicia – Tras-os-Montes). Tesis de Licenciatura. Universidad Complutense Madrid, 163 pp.

Rubio Pascual, F., Arenas, R. and Díaz García F. 1993. Evolución tectonotermal de la Unidad Santiago (Complejo de Ordenes): Un ejemplo de subducción eo-hercínica y descompresión sin-colisional. *Geogaceta,* 13.

Smye, A.J., Greenwood, L.V. and Holland, T.J.B. 2010. Garnet-chloritoid-kyanite assemblages: eclogite facies indicators of subduction constraints in orogenic belts. *Journal of Metamorphic Geology*, 28, 753–768.

Spear, F. and Menard, T. 1989. Programm GIBBS: A generalized Gibbs method algorithm. *American Mineralogist,* 74, 942–943.

Symmes, G. and Ferry, J. 1992. The effect of whole-rock MnO contento n the stability of garnet in pelitic schists during metamorphism. Journal of Metamorphic *Geology*, 27, 153–164.

Thompson, A. and England, P. 1984. Pressure-Temperature-Time Paths of Regional Metamorphism II. Their inference and interpretation using Mineral Assemblages in Metamorphics rocks. *Journal of Petrology*, 25 (4): 929–955.

Tracy, R.J. 1982, Compositional zoning and inclusions in metamorphic minerals, in Ferry, J.M., ed., Characterization of metamorphism through mineral equilibria. *Mineralogical Society of America Reviews in Mineralogy,* 10, 355–397.

Tuccillo, M., Essene, E. and van der Pluijm, D. 1990. Growth and retrograde zoning in garnets from high-grade metapelites: Implications for pressure-temperature paths. *Geology*, 18, 839–842.

Turner, F. 1981. Metamorphic petrology, mineralogical, field and tectonic aspects. 2nd edition. McGraw–Hill, New York. 524 pp.

Vernon R. and Clarke, G. 2008. Principles of Metamorphic Petrology. Cambridge University Press, New York, 446 pp.

Viereck, L., Flower M., Hertogen, J., Schmincke, H. and

Jenner, G. 1989. The genesis and significance of N–MORB sub–types. *Contributions to Mineralogy and Petrology,* 102, 112–126.

Von Raumer, J.F. and Stampfli, G.M. 2008. The birth of the Rheic Ocean–Early Palaeozoic subsidence patterns and subsequent tectonic plate scenarios. *Tectonophysics,* 46, 9-20.

Waters, D. 2004. Practical Aspects of Mineral Thermobarometry. Recuperado el 02 de mayo de 2017 de: http://www.earth.ox.ac.uk/~davewa/pt/index.html

White, R.W., Powell, R. and Johnson, T.E. 2014a. The effect of Mn on mineral stability in metapelites revisited: new a-x relations for manganese-bearing minerals. *Journal of Metamorphic Geology*, 32, 809–828.

White, R.W., Powell, R., Holland, T.J.B. and Worley, B. 2000. The effect of TiO_2 and Fe_2O_3 on metapelitic assemblages at greenschist and amphibolite facies conditions: mineral equilibria calculations in the system $K2O–FeO–MgO–Al_2O_3–SiO_2–H_2O–TiO_2–Fe_2O_3$. *Journal of Metamorphic Geology*, 18, 497–511.

White, R.W., Powell, R., Holland, T.J.B., Johnson, T.E. and Green, E.C.R. 2014b. New mineral activity-composition relations for thermodynamic calculations in metapelitic systems. *Journal of Metamorphic Geology*, 32, 261–286.

Yardley, B. 1977. An empirical study of diffusion in garnet. *American Mineralogist*, 62, 793–800.

Yardley, B. 1989. *An Introduction to Metamorphic Petrology*, Longman Earth Science Series, London, 248 pp.